

Nested hyperedges promote the onset of collective transitions but suppress explosive behavior

Federico Malizia,^{1,*} Andrés Guzmán,² Federico Battiston,¹ and István Z. Kiss^{2,3,†}

¹*Department of Network and Data Science, Central European University, Vienna, Austria*

²*Network Science Institute, Northeastern University London, London E1W 1LP, United Kingdom*

³*Department of Mathematics, Northeastern University, Boston, MA 02115, USA*

(Dated: January 16, 2026)

Higher-order interactions can dramatically reshape collective dynamics, yet how their microscopic organization controls macroscopic critical behavior remains unclear. Here we develop a new theory to study contagion dynamics on hypergraphs and show that nested hyperedges not only facilitate the onset of spreading, but also suppress backward bifurcations, thereby inhibiting explosive behavior. By disentangling contagion pathways, we find that overlap redirects transmission from external links to internal, group-embedded routes—boosting early activation but making dyadic and triadic channels increasingly redundant. This loss of structural independence quenches the nonlinear amplification required for bistability, progressively smoothing the transition as hyperedges become nested. We observe the same phenomenology in Kuramoto dynamics, pointing to a broadly universal mechanism by which nested higher-order structure governs critical transitions in complex systems.

Introduction— Higher-order interactions enrich the collective behavior of complex systems, enabling multistability, hysteresis, and discontinuous transitions [1–9]. Recent work has clarified, however, that these effects depend not only on the *presence* of higher-order interactions, but also on their *microscopic* organization [10–17]—i.e. how group interactions are arranged and correlated across the system. In particular, it has been observed that intra-order correlations can suppress explosive behavior by reducing the effective reinforcement among groups of the same size [11]. Cross-order correlations, instead, have been shown to shift the epidemic onset [13–15] and to drive the system along different pathways to explosive contagion [15]. Despite these observations, our understanding of why group interaction patterns influence the onset and nature of overall dynamics remains unknown.

Here, we show that nested hyperedges—an ubiquitous feature of real-world systems [18–21]—not only anticipate the onset of collective transitions [13, 15] in higher-order processes, but are also responsible for suppressing backward bifurcations—thereby inhibiting explosive behavior. We develop a microscopic theory for higher-order SIS dynamics, and show that nestedness systematically reallocates transmission from external links to group-embedded routes, anticipating the epidemic onset while progressively reducing the structural independence between dyadic and triadic channels. This loss of independence weakens the nonlinear feedback required for bistability, providing a microscopic dynamical explanation for the disappearance of backward bifurcations and explosive transitions in nested hypergraphs. Our findings extend beyond contagion dynamics, to higher-order synchronization processes, pointing towards a universal mechanism by which the microscopic structural organization of higher-order interactions governs the emergence of collective behavior.

Modeling nestedness in higher-order contagion.— We consider a hypergraph $\mathcal{H} = (\mathcal{N}, \mathcal{E})$ with N nodes and hyperedges

representing group interactions. Each hyperedge $e \in \mathcal{E}$ has order $m = |e| - 1$, with $m = 1$ corresponding to pairwise interactions and $m = 2$ to three-body interactions. We focus on systems with maximum order $M = 2$ and assume a regular structure in which each node participates in exactly k_1 links and k_2 2-hyperedges.

To quantify cross-order structural correlations, we use the *inter-order hyperedge overlap* [12], $\alpha = |\mathcal{E}_1 \cap \mathcal{F}(\mathcal{E}_2)| / |\mathcal{F}(\mathcal{E}_2)|$, where \mathcal{E}_1 and \mathcal{E}_2 are the sets of 1- and 2-hyperedges and $\mathcal{F}(\mathcal{E}_2)$ is the set of 1-cliques contained within the 2-hyperedges. Thus $\alpha \in [0, 1]$ measures the fraction of dyadic interactions structurally embedded within triadic ones, ranging from independent layers ($\alpha = 0$) to a fully nested (simplicial) structure ($\alpha = 1$).

We study a Susceptible–Infected–Susceptible (SIS) process: a susceptible node is infected through a 1-hyperedge at rate β_1 or through a 2-hyperedge with two infected neighbors at rate β_2 , and recovers at rate μ . To capture the effect of nestedness on dynamical correlations, we develop a homogeneous mean-field framework that tracks node, pair, and group-state densities, overcoming the limitations of pair-based [22, 23] and motif-based [13] approaches by explicitly incorporating inter-order overlap α , in the spirit of [15].

The density of infected individuals evolves as

$$\dot{\rho}^I = -\mu\rho^I + \beta_1 k_1 \rho^{SI} + \beta_2 k_2 \rho^{ISI\Delta}, \quad (1)$$

where ρ^{SI} is the density of *SI* links and $\rho^{ISI\Delta}$ is the density of 2-hyperedges composed of one susceptible and two infected nodes. These coevolve with $(\rho^{SSS\Delta}, \rho^{SSI\Delta})$, yielding a closed dynamical system $\dot{\mathbf{x}} = \mathbf{F}(\mathbf{x})$ for $\mathbf{x} = (\rho^I, \rho^{SI}, \rho^{SSS\Delta}, \rho^{SSI\Delta}, \rho^{ISI\Delta})$. Using conservation relations within node, pair, and group variables, we recover $\rho^S = 1 - \rho^I$, $\rho^{II} = \rho^I - \rho^{SI}$, and $\rho^{III\Delta} = 1 - \rho^{SSS\Delta} - 3\rho^{SSI\Delta} - 3\rho^{ISI\Delta}$.

The overlap parameter α directly shapes the evolution of pair and group states by controlling how many of the k_1 dyadic contacts of a node are shared within 2-hyperedges. When $\alpha = 0$, pairwise and triadic interactions act as independent contagion channels; when $\alpha = 1$, all links are embedded

* maliziaf@ceu.edu

† istvan.kiss@nulondon.ac.uk

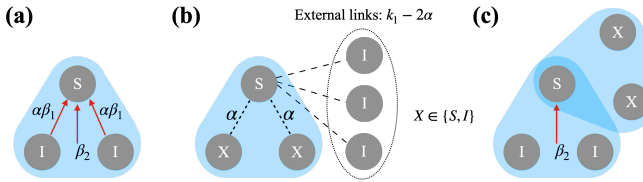


FIG. 1. **Higher-order contagion with nested hyperedges.** (a) Schematic of a 2-hyperedge in state $\rho^{ISI\Delta}$ (two infected and one susceptible node). The inter-order overlap α weights the contribution of pairwise infections occurring on links embedded within 2-hyperedges (internal channel), relative to infections occurring on external links. (b) Illustration of the local neighborhood of a susceptible node participating in k_2 2-hyperedges. Increasing overlap increases the number of pairwise contacts that are internal to the groups and reduces the number of external links available for transmission. (c) Example configuration in which a susceptible node is shared by two 2-hyperedges, one of which contains two infected nodes, highlighting how overlap couples dyadic and triadic transmission pathways.

in groups, so dyadic and triadic pathways are maximally coupled and effectively act on the same local neighborhood.

A key consequence of overlap is that it redistributes external- and inside-pairwise interactions within each group interaction. For a node participating in a given 2-hyperedge, the fully nested limit implies that two of its k_1 links are already “used” as within-group links, leaving $k_1 - 2$ external links; in the non-nested limit, all k_1 links are external. We model intermediate overlap by interpolating between these extremes, yielding an effective number of external links available to a node *within a group context*, $(1 - \alpha)k_1 + \alpha(k_1 - 2) = k_1 - 2\alpha$, which is the structural lever through which nestedness couples pair and group motifs (Fig. 1). Operationally, $k_1 - 2\alpha$ enters whenever a transition requires an *external* infected neighbor while the focal susceptible node is already conditioned on being part of a 2-hyperedge. The evolution equations of the state variables form a hierarchy involving motifs of increasing order. To obtain a closed system, higher-order terms are expressed in terms of lower-order correlations via standard mean-field closures [24, 25]. For tractability, we neglect correlations within each interaction order (no closed triples of links and negligible intra-order overlap among distinct 2-hyperedges) [11]; this removes clustering effects while preserving the cross-order correlations controlled by α . In this setting, a susceptible node already in a link has $(k_1 - 1)$ remaining links, and we approximate the probability that it connects to a neighbor in state $X \in \{S, I\}$ as $\rho^{SX}\rho^{SI}/\rho^S$. Similarly, a susceptible node already in a 2-hyperedge belongs to $(k_2 - 1)$ additional 2-hyperedges, and the probability that it connects externally to a 2-hyperedge with two infected nodes is approximated as $\rho^{XSX\Delta}\rho^{ISI\Delta}/\rho^S$. Crucially, when link-mediated infection is evaluated *in the context of a group*, external-link contributions to both pair and group equations are weighted by the reduced factor $k_1 - 2\alpha$. Accordingly, the probability that a susceptible node within a group is connected to an infected node via a 1-hyperedge is given by $\rho^{XSX\Delta}\rho^{SI}/\rho^S$. A pictorial representation of the corresponding

motifs is shown in Fig. 1. The full closed system is reported in the Appendix.

Nested hyperedges promote the onset of collective transitions but suppress explosive behavior— We now quantify how overlap shapes both the epidemic onset and the emergence of bistability. We use the rescaled infectivities $\lambda_1 = k_1\beta_1/\mu$ and $\lambda_2 = k_2\beta_2/\mu$, and denote by λ_1^* the transcritical threshold and by $\hat{\lambda}_2$ the minimum group infectivity required for a backward bifurcation (bistability).

We linearize around the disease-free equilibrium $\mathbf{x}^* = (0, 0, 1, 0, 0)$ and determine the epidemic threshold from the leading eigenvalue of the Jacobian (Appendix). The critical value λ_1^* can be obtained analytically as the solution of a quadratic equation arising from the linear stability condition. However, due to the complexity of the expression, the dependence of λ_1^* on model parameters is not obvious. To extract the leading structural dependence, we perform an asymptotic expansion for small overlap α , obtaining

$$\lambda_1^* \approx \frac{k_1}{k_1 - 1} - \alpha\lambda_2 \frac{k_1^2}{(k_1 - 1)^3}. \quad (2)$$

This expression shows that nestedness anticipates the epidemic onset through the combined control $\alpha\lambda_2$, while recovering the standard SIS threshold on networks, $\lambda_1^{*,(0)} = k_1/(k_1 - 1)$, in the non-nested limit $\alpha = 0$ [24]. This behavior is consistent with previous results on higher-order contagion [13, 15]. To determine the *type* of transition, we perform a center-manifold reduction [26, 27]. Near the epidemic threshold, the dynamics reduces to the normal form

$$\dot{u} = h u^2 + z \phi u + \mathcal{O}(u^3, \phi u^2), \quad (3)$$

where $\phi = \lambda_1 - \lambda_1^*$ measures the distance from criticality. The coefficients h and z are given by standard projections of the nonlinear vector field onto the critical eigenspace of the Jacobian (see Appendix), and quantify, respectively, the leading nonlinear self-interaction and the linear unfolding of the instability. We find that $z > 0$ at criticality; therefore, the direction of the bifurcation is entirely controlled by the sign of h : $h < 0$ yields a supercritical (continuous) transition, while $h > 0$ implies a subcritical (backward) bifurcation with bistability and explosive onset. Although the nonlinear coefficient h can be obtained analytically as a rational function implicitly depending on the critical point λ_1^* and the model parameters, its dependence on the key control parameters is not straightforward. Consequently, the bistability threshold $\hat{\lambda}_2$ is determined numerically. Nevertheless, inspecting the full expansion of the nonlinear coefficient shows that h depends nonlinearly on both the overlap α and the critical pairwise infectivity λ_1^* , with contributions up to fourth order in α . These terms encode competing reinforcing and suppressing effects arising from pairwise and group interactions.

Figure 2(a) shows that h decreases monotonically with α for $k_1 = 5$, $k_2 = 2$ and $\lambda_2 \in \{1, 2, 3, 4\}$, identifying a critical overlap α_c where $h = 0$ (dashed): increasing nestedness

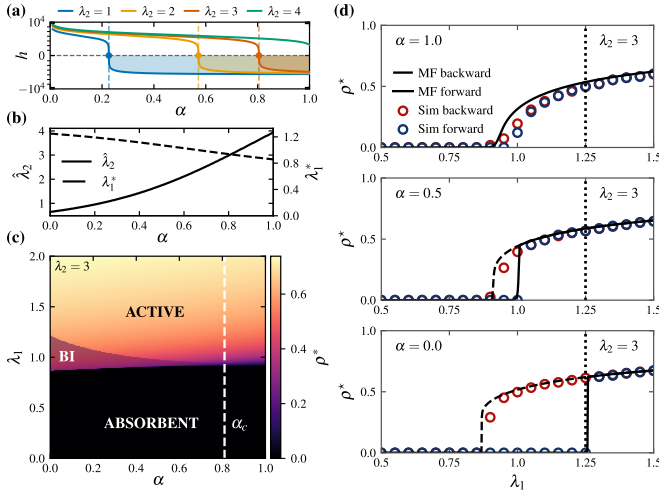


FIG. 2. Nested hyperedges promote the onset of collective transitions but suppress explosive behavior. (a) Nonlinear coefficient a from center-manifold theory as a function of overlap α , for $\lambda_2 \in \{1, 2, 3, 4\}$ (with $k_1 = 5, k_2 = 2$). Vertical dashed lines mark the critical overlap α_c at which $h = 0$ and the transition changes from subcritical (bistable) to supercritical (continuous). (b) Critical three-body infectivity $\hat{\lambda}_2$ (solid) required for bistability and the corresponding epidemic threshold λ_1^* (dashed), both obtained numerically as functions of α for $k_1 = 5, k_2 = 2$. (c) Phase diagram in the (α, λ_1) plane predicted by the model for $k_1 = 5, k_2 = 2$, and $\lambda_2 = 3$, showing that increasing α lowers λ_1^* while shrinking the bistable region, which disappears for $\alpha > \alpha_c$, yielding continuous transitions. (d) Stationary infected density ρ^* from theory (lines) and Gillespie simulations (markers) on random regular hypergraphs with $N = 3000, k_1 = 5$, and $k_2 = 2$, for three representative values of α at $\lambda_2 = 3$. For $\alpha = 1$, forward and backward branches coincide (continuous transition); for $\alpha = 0.5$, bistability emerges (forward: solid/blue; backward: dashed/red); for $\alpha = 0$, bistability is maximal and the forward threshold occurs at $\lambda_1^{*,(0)}$ (vertical dotted lines).

weakens the nonlinear amplification needed to sustain bistability and eventually turns a backward bifurcation into a continuous onset. For $\lambda_2 = 4$, h remains positive over $\alpha \in [0, 1]$, indicating that bistability survives even at strong overlap, although it is progressively weakened. Together with Eq. (2), this already reveals the dual role of overlap: it lowers λ_1^* while pushing the system away from the subcritical regime.

For $\alpha = 0$, the condition for bistability simplifies to:

$$\hat{\lambda}_2^{(0)} = \frac{(k_1 - 1)^2}{k_1^2}. \quad (4)$$

Thus, when dyadic and triadic interactions are uncorrelated, the onset of the backward bifurcation is controlled solely by the pairwise connectivity k_1 . Notably, sparse pairwise layers favor explosive behavior at smaller λ_2 .

To validate these predictions, we run Gillespie simulations on random regular hypergraphs with controlled α . Starting from hypergraphs with fully nested hyperedges ($\alpha = 1$), we rewire the 1-hyperedge layer while preserving its degree sequence to generate ensembles spanning $\alpha \in [0, 1]$ (SM). Figure 2(b) reports $\hat{\lambda}_2(\alpha)$ (from $h = 0$) together with the cor-

responding $\lambda_1^*(\alpha)$ (from the Jacobian), showing that $\hat{\lambda}_2$ increases while λ_1^* decreases with overlap. Figure 2(c) summarizes the stationary states of infected densities $\rho^* \equiv \rho^I$ in the (λ_1, α) space, at $\lambda_2 = 3$: the bistable region shrinks with α and vanishes at α_c . Figure 2(d) shows $\rho^*(\lambda_1)$ for representative α , in good agreement with simulations; small discrepancies at large α are consistent with overlap-induced pairwise clustering in sparse hypergraphs, neglected by our closure [28, 29]. The same qualitative phenomenology is observed in Kuramoto dynamics (see SM): increasing nestedness anticipates the onset of synchronization while suppressing the explosive transitions typically induced by higher-order interactions [30].

Microscopic mechanisms underlying the anticipated onset and suppressed bistability.— Having established that overlap facilitates spreading onset but suppresses bistability, we now identify the microscopic mechanism responsible for the observed phenomena. From Eq. (1), the infected population grows whenever

$$\left(\lambda_1 + \lambda_2 \frac{\rho^{\text{ISI}\Delta}}{\rho^{\text{SI}}} \right) \frac{\rho^{\text{SI}}}{\rho^I} > 1. \quad (5)$$

The ratios $\Pi = \rho^{\text{SI}}/\rho^I$ and $\delta = \rho^{\text{ISI}\Delta}/\rho^{\text{SI}}$ act as *fast variables* [23, 31]: they relax on a much shorter timescale than ρ^I and rapidly approach quasi-stationary values at early times (SM). We denote these by $\bar{\Pi}$ and $\bar{\delta}$ and also introduce $\Psi = \delta \Pi = \rho^{\text{ISI}\Delta}/\rho^I$.

At early times ($t \rightarrow 0$, disease-free state), the transcritical (forward) threshold can be expressed as

$$\lambda_1^* = \frac{1}{\bar{\Pi}} - \lambda_2 \bar{\delta}. \quad (6)$$

Thus, higher-order interactions impact the epidemic threshold through the early-stage ratio $\rho^{\text{ISI}\Delta}/\rho^{\text{SI}}$. Although λ_1^* has a quadratic form, the quasi-stationary fast variables can be obtained analytically as implicit functions of λ_1^* (SM),

$$\begin{aligned} \bar{\delta} &= \frac{\alpha k_2 \lambda_1^{*2} (k_1 - 2\alpha)}{k_1 [k_1 k_2 - \alpha \lambda_1^* \lambda_2 (k_2 - 1)]} \\ \bar{\Pi} &= \frac{k_1}{2k_1 - \lambda_1^* (k_1 - 2) + \lambda_2 (4\alpha - k_1) \bar{\delta}}. \end{aligned} \quad (7)$$

In particular, $\bar{\delta} = 0$ at $\alpha = 0$, confirming that three-body contagion does not contribute at early times without overlap. Combining Eqs. (6) and (7) recovers the same critical condition obtained from linear stability of the full system.

To further isolate pairwise and three-body contributions, we disentangle the infected density as

$$\begin{aligned} \rho_1^I &= -\mu \rho_1^I + \beta_1 k_1 \rho^{\text{SI}}; \\ \rho_2^I &= -\mu \rho_2^I + \beta_2 k_2 \rho^{\text{ISI}\Delta}, \end{aligned} \quad (8)$$

where ρ_1^I and ρ_2^I are the contributions arising from pairwise and three-body transmission, respectively (and analogous decompositions can be written for other motif variables).

Moreover, pairwise transmission can be split into external versus group-embedded events by exploiting the group-state equations. As an illustrative example, for $\rho_1^{\text{ISI}_\Delta}$ we obtain

$$\begin{aligned}\dot{\rho}_{1,\text{ext}}^{\text{ISI}_\Delta} &= +\mu \left(\rho_{1,\text{ext}}^{\text{III}_\Delta} - 2\rho_{1,\text{ext}}^{\text{ISI}_\Delta} \right) \\ &\quad + \beta_1 (k_1 - 2\alpha) (2\rho^{\text{ISS}_\Delta \text{I}} - \rho^{\text{IIS}_\Delta \text{I}}) ; \\ \dot{\rho}_{1,\text{int}}^{\text{ISI}_\Delta} &= +\mu \left(\rho_{1,\text{int}}^{\text{III}_\Delta} - 2\rho_{1,\text{int}}^{\text{ISI}_\Delta} \right) + 2\alpha\beta_1 (\rho^{\text{SSI}_\Delta} - 2\rho^{\text{ISI}_\Delta}) .\end{aligned}\quad (9)$$

Within this framework, we derive a closed description of the early-time dynamics of the fast variables and their disentangled components by applying the chain rule to their defining ratios and evaluating them near the disease-free state (Appendix).

Figure 3(a) compares these theoretical predictions, obtained by numerically integrating the fast-variable equations (Appendix), with the corresponding estimates from Gillespie simulations, including the disentangled contributions. We estimate $\bar{\Pi}$ and $\bar{\delta}$ in Gillespie simulations by initializing with a single infected node close to λ_1^* and averaging over 5000 realizations in the early-time window $0.005 < \rho^1(t) < 0.01$. Theory and simulations agree well, particularly for the higher-order contribution $\bar{\Pi}_2$ and for the internal pairwise component $\bar{\delta}_{1,\text{(int)}}$; residual discrepancies for $\bar{\Pi}_1$ are consistent with finite-size fluctuations at very low densities. Crucially, both approaches show that the only nonvanishing contribution to $\bar{\delta}$ originates from *internal* pairwise contagion within groups, and that it increases monotonically with α . This directly explains the anticipated transcritical onset via Eq. (6): overlap promotes mixed group configurations with two infected and one susceptible node already near the disease-free state, increasing $\rho^{\text{ISI}_\Delta}/\rho^{\text{SI}}$.

Figures 3(b)-(c) connect this early-time mechanism to the stationary regime by decomposing ρ^* into total, pairwise (1-hyperedge), and group-based (2-hyperedge) contributions for $\alpha = 0$ and $\alpha = 1$ at their respective $\hat{\lambda}_2$ values. In both cases the transition is continuous, although for $\alpha = 1$ the system shows a sharper growth. For $\alpha = 0$, the endemic state is mainly sustained by pairwise transmission; for $\alpha = 1$, enhanced internal pairwise activity increases the number of active 2-hyperedges, so higher-order events dominate at stationarity without inducing bistability.

To quantify the microscopic redistribution of transmission routes, we define η_1^* and η_2^* as the fractions of accumulated infection events up to stationarity occurring through pairwise and higher-order channels, and split $\eta_1^* = \eta_{1,\text{ext}}^* + \eta_{1,\text{int}}^*$ into external and group-embedded link events. Figure 3(d) shows that for $\alpha = 0$ the dynamics is dominated by external pairwise transmission ($\eta_{1,\text{ext}}^* \simeq 0.8$), whereas increasing α progressively suppresses external contagion in favor of internal pairwise and higher-order events, with η_2^* becoming dominant. Importantly, center-manifold theory simultaneously yields an increasing $\hat{\lambda}_2(\alpha)$: larger overlap requires stronger higher-order coupling to sustain bistability. Taken together, high overlap both reduces the pool of external links (through $k_1 - 2\alpha$) and aligns dyadic and triadic pathways onto

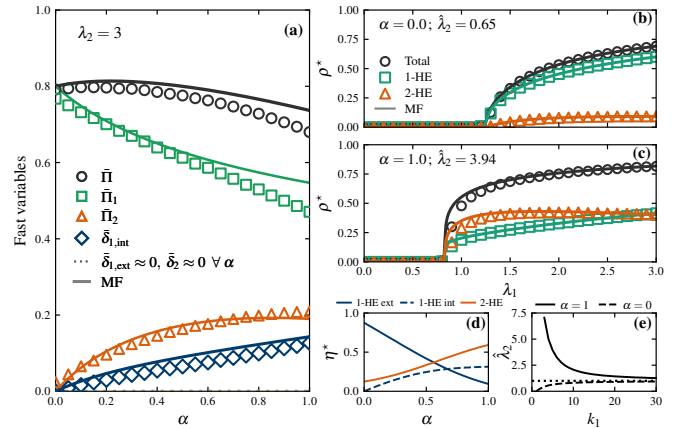


FIG. 3. Microscopic mechanisms underlying the anticipated onset and suppressed bistability. (a) Quasi-stationary states for the fast variables Π and δ as functions of the inter-order overlap α , obtained from theory (lines) and Gillespie simulations (symbols) on random regular hypergraphs with $N = 3000$, $k_1 = 5$, $k_2 = 2$, and $\lambda_2 = 3$. Each point is evaluated close to λ_1^* for each α . The only nonvanishing contribution to $\bar{\delta}$ arises from internal pairwise contagion within groups and increases with α . (b,c) Decomposition of the stationary infected density ρ^* into total, pairwise (1-hyperedge), and group-based (2-hyperedge) contributions for $\alpha = 0$ and $\alpha = 1$, evaluated at the corresponding critical values $\hat{\lambda}_2$, before bistability emerges. In both cases the transition remains continuous, although nested structures display a sharper onset. (d) Fractions of accumulated infection events η_1^* (pairwise, internal and external) and η_2^* (higher-order) near λ_1^* as functions of α , showing a progressive shift from external pairwise to internal and higher-order transmission channels. (e) Critical group infectivity $\hat{\lambda}_2$ versus k_1 (with $k_2 = 2$) for $\alpha = 0$ (dashed, analytical) and $\alpha = 1$ (solid, numerical), illustrating the strong suppression of explosive behavior induced by overlap in sparse networks; both curves converge to the mean-field limit $\hat{\lambda}_2 = 1$ (dotted line) for large k_1 .

essentially the same nodes, weakening the nonlinear amplification needed for a backward bifurcation and thereby suppressing explosive transitions even when higher-order events dominate.

Figure 3(e) further shows that this suppression is strongest in sparse structures. Comparing $\alpha = 0$ [Eq. (4)] with $\alpha = 1$ [obtained numerically from Eq.(3)], low k_1 dramatically increases the $\hat{\lambda}_2$ required for bistability, while increasing k_1 lowers $\hat{\lambda}_2$ by providing additional external links. In both cases $\hat{\lambda}_2 \rightarrow 1$ for large k_1 [3]. Equations (2) and (4) provide complementary intuition at $\alpha = 0$: sparse pairwise connectivity delays the forward transition by increasing λ_1^* and at the same time makes the system more susceptible to backward bifurcations. This is consistent with mean-field first-order phenomenology sustained by nonlinear feedback [32]. On the contrary, in nested hypergraphs, this behavior is flipped due to the presence of more *internal* links within groups (Fig. 3d), which decrease λ_1^* while making dyadic and triadic pathways increasingly redundant, thereby shrinking the bistable window and pushing $\hat{\lambda}_2$ upward.

Conclusions.— In this paper we showed that nestedness

across interaction orders simultaneously regulates epidemic onset and the nature of the transition. Combining a closed mean-field theory with center-manifold analysis and Gillespie simulations on hypergraphs with tunable inter-order overlap, we find a robust dual effect: increasing overlap anticipates the transcritical threshold while suppressing bistability and explosive (discontinuous) transitions by raising the critical group infectivity required for a saddle-node bifurcation. A fast-variables analysis identifies the microscopic origin of the anticipated onset, revealing that overlap selectively amplifies internal pairwise contagion within groups and enhances the early formation of mixed group configurations near the disease-free state. At the same time, overlap reduces the structural independence between dyadic and triadic transmission channels, weakening the nonlinear amplification needed for explosive behavior—most strongly in sparse higher-order networks. Our results extend beyond spreading phenomena: in the SM we show that for synchronization processes, in particular higher-order Kuramoto dynamics, nested hyperedges anticipate the onset of synchronization while suppressing explosive synchronization. Taken together, our findings indicate that the microscopic organization of higher-order interactions provides a universal structural control over both the onset and the nature of collective nonlinear phenomena, enriching our understanding of networked dynamics beyond pairwise interactions.

Appendix A: Homogeneous mean-field model and closures.— We consider SIS dynamics on a regular hypergraph with pairwise (1-hyperedges) and three-body (2-hyperedges) interactions. Susceptible nodes become infected either through a link at rate β_1 or through a 2-hyperedge with two infected neighbors at rate β_2 , while infected nodes recover at rate μ . The microscopic nestedness between the two interaction orders is controlled by the inter-order overlap α .

We track the state vector $\mathbf{x} = (\rho^I, \rho^{SI}, \rho^{SSS\Delta}, \rho^{SSI\Delta}, \rho^{ISI\Delta})$, where $\rho^A = [A]/N$, $\rho^{AB} = [AB]/(Nk_1)$, and $\rho^{ABC\Delta} = [ABC\Delta]/(2Nk_2)$ denote normalized motif densities (node, link, and 2-hyperedge states, respectively). By homogeneity and permutation symmetry, $\rho^{SI} = \rho^{IS}$ and, e.g., $\rho^{ISI\Delta} = \rho^{IIS\Delta} = \rho^{SII\Delta}$. Additionally, we define densities for higher-order composite motifs as follows. Let ρ^{ABC} denote the density of pairs of links that share a common node, where the nodes are in states A, B (the shared node), and C. Let $\rho^{ABC\Delta D}$ denote the density of 2-hyperedges whose nodes are in states A, B, and C, with the additional constraint that the node in state C also participates in a link with a node in state D. Finally, let $\rho^{ABCDE\bowtie}$ denote the density of 2-hyperedges whose nodes are in states A, B, and C, where the node in state C is also part of another 2-hyperedge with nodes in states D and E.

The dynamics reads

$$\begin{aligned}
\dot{\rho}^I &= -\mu\rho^I + \beta_1 k_1 \rho^{SI} + \beta_2 k_2 \rho^{ISI\Delta}; \\
\dot{\rho}^{SI} &= \beta_1 [(k_1 - 1)(\rho^{SSI} - \rho^{ISI}) - \rho^{SI}] \\
&\quad + \beta_2 \frac{k_2}{k_1} [(k_1 - 2\alpha)(\rho^{IIS\Delta S} - \rho^{IIS\Delta I}) - 2\alpha\rho^{ISI\Delta}] \\
&\quad + \mu(\rho^{II} - \rho^{SI}); \\
\dot{\rho}^{SSS\Delta} &= -3\beta_1(k_1 - 2\alpha)\rho^{SSS\Delta I} - 3\beta_2(k_2 - 1)\rho^{SSSII\bowtie} \\
&\quad + 3\mu\rho^{SSI\Delta}; \\
\dot{\rho}^{SSI\Delta} &= \beta_1 [(k_1 - 2\alpha)(\rho^{SSS\Delta I} - 2\rho^{ISS\Delta I}) - 2\alpha\rho^{SSI\Delta}] \\
&\quad + \beta_2(k_2 - 1)(\rho^{SSSII\bowtie} - 2\rho^{ISSII\bowtie}) \\
&\quad + \mu(2\rho^{ISI\Delta} - \rho^{SSI\Delta}); \\
\dot{\rho}^{ISI\Delta} &= \beta_1 [(k_1 - 2\alpha)(2\rho^{ISS\Delta I} - \rho^{IIS\Delta I})] \\
&\quad + 2\alpha\beta_1(\rho^{SSI\Delta} - \rho^{ISI\Delta}) \\
&\quad + \beta_2[(k_2 - 1)(2\rho^{ISSII\bowtie} - \rho^{IISII\bowtie}) - \rho^{ISI\Delta}] \\
&\quad + \mu(\rho^{III\Delta} - 2\rho^{ISI\Delta}),
\end{aligned} \tag{10}$$

The remaining densities entering Eq. (10) are recovered through consistency identities (holding separately for link and 2-hyperedge state spaces), namely $\rho^S = 1 - \rho^I$, $\rho^{II} = \rho^I - \rho^{SI}$, $\rho^{SS} = \rho^S - \rho^{SI}$, and $\rho^{III\Delta} = 1 - \rho^{SSS\Delta} - 3\rho^{SSI\Delta} - 3\rho^{ISI\Delta}$. The factors proportional to α account for infection events occurring through links embedded in 2-hyperedges. Moreover, the combination $k_1 - 2\alpha$ represents the expected number of *external* links available to a node that belongs to a 2-hyperedge, since overlap consumes two dyadic contacts inside each group.

To close the hierarchy, we neglect (i) closed triples of links (no triangular clustering in the pairwise layer) and (ii) intra-order overlap among distinct 2-hyperedges (see also Ref. [13]). Under these assumptions, higher-order composite motifs factorize into products of lower-order densities, yielding

$$\begin{aligned}
\rho^{ISI} &= \frac{(\rho^{SI})^2}{\rho^S}, & \rho^{SSI} &= \frac{\rho^{SS}\rho^{SI}}{\rho^S}, \\
\rho^{SSS\Delta} &= \frac{\rho^{SSS\Delta}\rho^{SI}}{\rho^S}, & \rho^{ISS\Delta I} &= \frac{\rho^{SSI\Delta}\rho^{SI}}{\rho^S}, \\
\rho^{IIS\Delta S} &= \frac{\rho^{ISI\Delta}\rho^{SS}}{\rho^S}, & \rho^{IIS\Delta I} &= \frac{\rho^{ISI\Delta}\rho^{SI}}{\rho^S}, \\
\rho^{ISSII\bowtie} &= \frac{\rho^{SSI\Delta}\rho^{ISI\Delta}}{\rho^S}, & \rho^{SSSII\bowtie} &= \frac{\rho^{SSS\Delta}\rho^{ISI\Delta}}{\rho^S}, \\
\rho^{IISII\bowtie} &= \frac{(\rho^{ISI\Delta})^2}{\rho^S}.
\end{aligned} \tag{11}$$

To determine the onset of spreading, we introduce the rescaled infectivities $\lambda_1 = k_1\beta_1/\mu$ and $\lambda_2 = k_2\beta_2/\mu$ and linearize Eqs. (10) around the disease-free equilibrium $\mathbf{x}^* =$

$(0, 0, 1, 0, 0)$. The epidemic threshold (transcritical bifurcation) is obtained by imposing that the dominant eigenvalue of the Jacobian crosses zero. For compactness, we define $\Gamma(\lambda_1) \equiv k_1 - (k_1 - 1)\lambda_1$ and $\Theta(\alpha, \lambda_1) \equiv k_1 k_2 + (k_1 + k_2 - 1)\lambda_1 - k_1 - 4\alpha k_2 \lambda_1$, which yields the exact condition

$$\alpha \lambda_1 \lambda_2 \left[4\alpha^2 k_2 \lambda_1 + k_1 \Theta(\alpha, \lambda_1) \right] = k_1^2 k_2 \Gamma(\lambda_1). \quad (12)$$

Appendix B: Center-manifold reduction.— To characterize the *type* of transition at the epidemic threshold, we perform a center-manifold reduction of the closed system $\dot{\mathbf{x}} = \mathbf{F}(\mathbf{x}; \lambda_1, \lambda_2, \alpha)$ about the disease-free equilibrium $\mathbf{x}^* = (0, 0, 1, 0, 0)$. The critical point is defined implicitly by Eq. (12); throughout, all quantities below are evaluated on this critical manifold. Let $J = D_{\mathbf{x}} \mathbf{F}(\mathbf{x}^*; \lambda_1, \lambda_2, \alpha)|_{\text{crit}}$ be the Jacobian at criticality and let \mathbf{w} and \mathbf{v} denote the right and left eigenvectors associated with the simple zero eigenvalue, normalized by $\mathbf{v}^\top \mathbf{w} = 1$. Introducing the unfolding parameter $\phi = \lambda_1 - \lambda_1^*$ (with λ_1^* defined implicitly by Eq. (12)), the dynamics on the center manifold reduces to the scalar normal form $\dot{u} = hu^2 + z\phi u + \mathcal{O}(u^3, \phi u^2)$.

In terms of the vector field \mathbf{F} , the quadratic coefficient is

$$h = \sum_{i,j,k=1}^b v_i \frac{\partial^2 F_i}{\partial x_j \partial x_k}(\mathbf{x}^*; \lambda_1, \lambda_2, \alpha) \Big|_{\phi=0} w_j w_k, \quad (13)$$

and the parameter-dependent coefficient is

$$z = \sum_{i,j=1}^b v_i \frac{\partial^2 F_i}{\partial x_j \partial \lambda_1}(\mathbf{x}^*; \lambda_1, \lambda_2, \alpha) \Big|_{\phi=0} w_j, \quad (14)$$

with $b = \dim(\mathbf{x}) = 5$.

Appendix C: Fast-variable system.— In the early stage ($\rho^I \rightarrow 0$), ratios of motif densities relax on a fast time scale. We define the fast variables $\Pi \equiv \rho^{SI}/\rho^I$ and $\Psi \equiv \rho^{ISI\Delta}/\rho^I$, so that $\delta \equiv \rho^{ISI\Delta}/\rho^{SI} = \Psi/\Pi$ (main text). To close the fast-variable dynamics we introduce two additional ratios, $\Omega \equiv \rho^{SSS\Delta}/\rho^I$ and $\Upsilon \equiv \rho^{SSI\Delta}/\rho^I$. The remaining pair fast variable is eliminated using the identity $\rho^{SI} + \rho^{II} = \rho^I$, i.e., $\rho^{II}/\rho^I = 1 - \Pi$. Fast-variable equations follow by differentiating ratios via the chain rule; e.g., $\dot{\Pi} = (\dot{\rho}^{SI}/\rho^I) - \Pi(\dot{\rho}^I/\rho^I)$, and similarly for Υ, Ψ, Ω .

Substituting the motif equations and closures into the chain-rule expressions yields

$$\begin{aligned} \dot{\Pi} &= \mu(1 - \Pi) + \beta_1(k_1 - 2)\Pi + \beta_2 \frac{k_2}{k_1}(k_1 - 4\alpha)\Psi \\ &\quad - \beta_1 k_1 \Pi^2 - \beta_2 k_2 \Pi \Psi, \\ \dot{\Upsilon} &= \beta_1(k_1 - 2\alpha)\Pi - 2\beta_1 \alpha \Upsilon + (2\mu + \beta_2(k_2 - 1))\Psi \\ &\quad - \beta_1 k_1 \Pi \Upsilon - \beta_2 k_2 \Upsilon \Psi, \\ \dot{\Omega} &= \mu(2\Upsilon + \Omega) - 3\beta_1(k_1 - 2\alpha)\Pi - 3\beta_2(k_2 - 1)\Psi \\ &\quad - \beta_1 k_1 \Pi \Omega - \beta_2 k_2 \Omega \Psi. \\ \dot{\Psi} &= 2\beta_1 \alpha \Upsilon + (-2\beta_1 \alpha - \mu - \beta_2)\Psi + \mu(1 - \Omega \\ &\quad - 3\Upsilon - 3\Psi) - \beta_1 k_1 \Pi \Psi - \beta_2 k_2 \Psi^2, \end{aligned} \quad (15)$$

This system directly provides the early-time evolution of $\Psi = \rho^{ISI\Delta}/\rho^I$ and hence of $\delta = \Psi/\Pi = \rho^{ISI\Delta}/\rho^{SI}$.

Appendix D: Disentangling by interaction order and internal/external pairwise channels.—We decompose the evolution equations for group-state densities in Eq. (10) by explicitly disentangling the microscopic processes that generate them. In particular, we separate the contributions arising from (i) genuine three-body infection events (subscript 2) and (ii) link-driven infection events, which are further split into pairwise transmission occurring on links that are internal to a group and on links external to it (subscripts 1, int and 1, ext, respectively).

Applying this disentangling to the group-state dynamics yields the following set of coupled equations:

$$\begin{aligned} \dot{\rho}_{1,\text{ext}}^{\text{SSS}\Delta} &= -3\beta_1(k_1 - 2\alpha)\rho^{\text{SSS}\Delta\text{I}} + 3\mu\rho_{1,\text{ext}}^{\text{SSI}\Delta} \\ \dot{\rho}_{1,\text{int}}^{\text{SSS}\Delta} &= +3\mu\rho_{1,\text{int}}^{\text{SSI}\Delta} \\ \dot{\rho}_2^{\text{SSS}\Delta} &= -3\beta_2(k_2 - 1)\rho^{\text{SSSII}\bowtie} + 3\mu\rho_2^{\text{SSI}\Delta} \\ \dot{\rho}_{1,\text{ext}}^{\text{SSI}\Delta} &= \beta_1[(k_1 - 2\alpha)(\rho^{\text{SSS}\Delta\text{I}} - 2\rho^{\text{ISS}\Delta\text{I}})] \\ &\quad + \mu(2\rho_{1,\text{ext}}^{\text{ISI}\Delta} - \rho_{1,\text{ext}}^{\text{SSI}\Delta}); \\ \dot{\rho}_{1,\text{int}}^{\text{SSI}\Delta} &= -2\beta_1 \alpha \rho^{\text{SSI}\Delta} + \mu(2\rho_{1,\text{int}}^{\text{ISI}\Delta} - \rho_{1,\text{int}}^{\text{SSI}\Delta}); \\ \dot{\rho}_2^{\text{SSI}\Delta} &= \beta_2(k_2 - 1)(\rho^{\text{SSSII}\bowtie} - 2\rho^{\text{ISSII}\bowtie}) \\ &\quad + \mu(2\rho_2^{\text{ISI}\Delta} - \rho_2^{\text{SSI}\Delta}); \\ \dot{\rho}_{1,\text{ext}}^{\text{ISI}\Delta} &= +\mu(\rho_{1,\text{ext}}^{\text{III}\Delta} - 2\rho_{1,\text{ext}}^{\text{ISI}\Delta}) \\ &\quad + \beta_1(k_1 - 2\alpha)(2\rho^{\text{ISS}\Delta\text{I}} - \rho^{\text{IIS}\Delta\text{I}}); \\ \dot{\rho}_{1,\text{int}}^{\text{ISI}\Delta} &= +\mu(\rho_{1,\text{int}}^{\text{III}\Delta} - 2\rho_{1,\text{int}}^{\text{ISI}\Delta}) + 2\alpha\beta_1(\rho^{\text{SSI}\Delta} - 2\rho^{\text{ISI}\Delta}); \\ \dot{\rho}_2^{\text{ISI}\Delta} &= +\mu(\rho_2^{\text{III}\Delta} - 2\rho_2^{\text{ISI}\Delta}) \\ &\quad + \beta_2[(k_2 - 1)(2\rho^{\text{ISSII}\bowtie} - \rho^{\text{IISII}\bowtie}) - \rho^{\text{ISI}\Delta}] \end{aligned}$$

Accordingly, the fast variables can be consistently decomposed into the sum of their higher-order, internal pairwise, and external pairwise contributions as

$$\begin{aligned} \Upsilon &= \Upsilon_2 + \Upsilon_{1,\text{int}} + \Upsilon_{1,\text{ext}}; \quad \Psi = \Psi_2 + \Psi_{1,\text{int}} + \Psi_{1,\text{ext}}; \\ \Omega &= \Omega_2 + \Omega_{1,\text{int}} + \Omega_{1,\text{ext}}. \end{aligned} \quad (16)$$

Denoting $\mathcal{L}(X) \equiv -\beta_1 k_1 \Pi X - \beta_2 k_2 \Psi X$, the disentan-

gled fast-variable dynamics reads

$$\begin{aligned}
\dot{\Upsilon}_2 &= 2\mu \Psi_2 + \beta_2(k_2 - 1)\Psi + \mathcal{L}(\Upsilon_2), \\
\dot{\Upsilon}_{1,\text{int}} &= 2\mu \Psi_{1,\text{int}} - 2\beta_1\alpha \Upsilon + \mathcal{L}(\Upsilon_{1,\text{int}}), \\
\dot{\Upsilon}_{1,\text{ext}} &= 2\mu \Psi_{1,\text{ext}} + \beta_1(k_1 - 2\alpha)\Pi + \mathcal{L}(\Upsilon_{1,\text{ext}}), \\
\dot{\Psi}_2 &= \mu(1 - \Omega_2 - 3\Upsilon_2 - 3\Psi_2) - \mu\Psi_2 \\
&\quad - \beta_2\Psi + \mathcal{L}(\Psi_2), \\
\dot{\Psi}_{1,\text{int}} &= \mu(1 - \Omega_{1,\text{int}} - 3\Upsilon_{1,\text{int}} - 3\Psi_{1,\text{int}}) \\
&\quad - \mu\Psi_{1,\text{int}} + 2\alpha\beta_1(\Upsilon - \Psi) + \mathcal{L}(\Psi_{1,\text{int}}), \quad (17) \\
\dot{\Psi}_{1,\text{ext}} &= \mu(1 - \Omega_{1,\text{ext}} - 3\Upsilon_{1,\text{ext}} - 3\Psi_{1,\text{ext}}) \\
&\quad - \mu\Psi_{1,\text{ext}} + \mathcal{L}(\Psi_{1,\text{ext}}), \\
\dot{\Omega}_2 &= \mu(2\Upsilon_2 + \Omega_2) - 3\beta_2(k_2 - 1)\Psi + \mathcal{L}(\Omega_2), \\
\dot{\Omega}_{1,\text{int}} &= \mu(2\Upsilon_{1,\text{int}} + \Omega_{1,\text{int}}) + \mathcal{L}(\Omega_{1,\text{int}}), \\
\dot{\Omega}_{1,\text{ext}} &= \mu(2\Upsilon_{1,\text{ext}} + \Omega_{1,\text{ext}}) - 3\beta_1(k_1 - 2\alpha)\Pi \\
&\quad + \mathcal{L}(\Omega_{1,\text{ext}}).
\end{aligned}$$

Equations (15)–(17) provide a closed early-time description of the fast variables, including the disentangled contributions by interaction order and by internal/external link channels within groups.

Acknowledgments.—F.M. acknowledges support from the Austrian Science Fund (FWF) through project 10.55776/PAT1652425. A.G. acknowledges the PhD studentship support from Northeastern University London. F.B. acknowledges support from the Austrian Science Fund (FWF) through project 10.55776/PAT1052824 and project 10.55776/PAT1652425.

[1] Federico Battiston, Giulia Cencetti, Iacopo Iacopini, Vito Latora, Maxime Lucas, Alice Patania, Jean-Gabriel Young, and Giovanni Petri. Networks beyond pairwise interactions: Structure and dynamics. *Physics reports*, 874:1–92, 2020.

[2] Federico Battiston, Enrico Amico, Alain Barrat, Ginestra Bianconi, Guilherme Ferraz de Arruda, Benedetta Franceschiello, Iacopo Iacopini, Sonia Kéfi, Vito Latora, Yamir Moreno, et al. The physics of higher-order interactions in complex systems. *Nature physics*, 17(10):1093–1098, 2021.

[3] Iacopo Iacopini, Giovanni Petri, Alain Barrat, and Vito Latora. Simplicial models of social contagion. *Nature communications*, 10(1):2485, 2019.

[4] Guilherme Ferraz de Arruda, Giovanni Petri, Pablo Martin Rodriguez, and Yamir Moreno. Multistability, intermittency, and hybrid transitions in social contagion models on hypergraphs. *Nature communications*, 14(1):1375, 2023.

[5] Per Sebastian Skardal and Alex Arenas. Higher order interactions in complex networks of phase oscillators promote abrupt synchronization switching. *Communications Physics*, 3(1):218, 2020.

[6] Andrea Civilini, Onkar Sadekar, Federico Battiston, Jesús Gómez-Gardeñes, and Vito Latora. Explosive cooperation in social dilemmas on higher-order networks. *Physical Review Letters*, 132(16):167401, 2024.

[7] Thomas Robiglio, Leonardo Di Gaetano, Ada Altieri, Giovanni Petri, and Federico Battiston. Higher-order ising model on hypergraphs. *Physical Review E*, 112(2):L022301, 2025.

[8] Christian Kuehn and Christian Bick. A universal route to explosive phenomena. *Science advances*, 7(16):eabe3824, 2021.

[9] Hugo Pérez-Martínez, Santiago Lamata-Otín, Federico Malizia, Luis Mario Floría, Jesús Gómez-Gardeñes, and David Soriano-Paños. Social polarization promoted by sparse higher-order interactions. *Communications Physics*, 2025.

[10] Yuanzhao Zhang, Maxime Lucas, and Federico Battiston. Higher-order interactions shape collective dynamics differently in hypergraphs and simplicial complexes. *Nature communications*, 14(1):1605, 2023.

[11] Federico Malizia, Santiago Lamata-Otín, Mattia Frasca, Vito Latora, and Jesús Gómez-Gardeñes. Hyperedge overlap drives explosive transitions in systems with higher-order interactions. *Nature communications*, 16(1):555, 2025.

[12] Santiago Lamata-Otín, Federico Malizia, Vito Latora, Mattia Frasca, and Jesús Gómez-Gardeñes. Hyperedge overlap drives synchronizability of systems with higher-order interactions. *Physical Review E*, 111(3):034302, 2025.

[13] Giulio Burgio, Sergio Gómez, and Alex Arenas. Triadic approximation reveals the role of interaction overlap on the spread of complex contagions on higher-order networks. *Physical Review Letters*, 132(7):077401, 2024.

[14] Jihye Kim, Deok-Sun Lee, and K-I Goh. Contagion dynamics on hypergraphs with nested hyperedges. *Physical Review E*, 108(3):034313, 2023.

[15] Federico Malizia, Andrés Guzmán, Iacopo Iacopini, and István Z Kiss. Disentangling the role of heterogeneity and hyperedge overlap in explosive contagion on higher-order networks. *Physical Review Letters*, 135(20):207401, 2025.

[16] Nicholas W Landry and Juan G Restrepo. The effect of heterogeneity on hypergraph contagion models. *Chaos: An Interdisciplinary Journal of Nonlinear Science*, 30(10), 2020.

[17] Leah A Keating and Laurent Hébert-Dufresne. Loops, not groups: Long cycles are responsible for discontinuous phase transitions in higher-order network contagions. *arXiv preprint arXiv:2511.15688*, 2025.

[18] Quintino Francesco Lotito, Federico Musciotto, Alberto Montresor, and Federico Battiston. Higher-order motif analysis in hypergraphs. *Communications Physics*, 5(1):79, 2022.

[19] Nicholas W Landry, Jean-Gabriel Young, and Nicole Eikmeier. The simpliciality of higher-order networks. *EPJ data science*, 13(1):17, 2024.

[20] Timothy LaRock and Renaud Lambiotte. Encapsulation structure and dynamics in hypergraphs. *Journal of Physics: Complexity*, 4(4):045007, 2023.

[21] Alec Kirkley, Helcio Felippe, and Federico Battiston. Structural reducibility of hypergraphs. *Physical Review Letters*, 135(24):247401, 2025.

[22] Federico Malizia, Luca Gallo, Mattia Frasca, István Z Kiss, Vito Latora, and Giovanni Russo. A pair-based approximation for simplicial contagion. *Chaos, Solitons & Fractals*, 199:116776, 2025.

[23] Matthew J Keeling. The effects of local spatial structure on epidemiological invasions. *Proceedings of the Royal Society of London. Series B: Biological Sciences*, 266(1421):859–867, 1999.

[24] István Z Kiss, Joel C Miller, Péter L Simon, et al. Mathematics of epidemics on networks. *Cham: Springer*, 598(2017):31, 2017.

[25] Thomas House, Geoffrey Davies, Leon Danon, and Matt J Keeling. A motif-based approach to network epidemics. *Bul-*

letin of Mathematical Biology, 71(7):1693–1706, 2009.

- [26] Carlos Castillo-Chavez and Baojun Song. Dynamical models of tuberculosis and their applications. *Math. Biosci. Eng.*, 1(2):361–404, 2004.
- [27] Yuri A Kuznetsov. *Elements of applied bifurcation theory*. Springer, 1998.
- [28] Joel C Miller. Spread of infectious disease through clustered populations. *Journal of the Royal Society Interface*, 6(41):1121–1134, 2009.
- [29] Joel C Miller. Percolation and epidemics in random clustered networks. *Physical Review E—Statistical, Nonlinear, and Soft Matter Physics*, 80(2):020901, 2009.
- [30] Per Sebastian Skardal and Alex Arenas. Abrupt desynchronization and extensive multistability in globally coupled oscillator simplexes. *Physical review letters*, 122(24):248301, 2019.
- [31] Rosanna C Barnard, Luc Berthouze, Péter L Simon, and István Z Kiss. Epidemic threshold in pairwise models for clustered networks: closures and fast correlations. *Journal of mathematical biology*, 79(3):823–860, 2019.
- [32] Uwe Thiele, Tobias Frohoff-Hülsmann, Sebastian Engelkemper, Edgar Knobloch, and Andrew J Archer. First order phase transitions and the thermodynamic limit. *New Journal of Physics*, 21(12):123021, 2019.
- [33] Juan A Acebrón, Luis L Bonilla, Conrad J Pérez Vicente, Félix Ritort, and Renato Spigler. The kuramoto model: A simple paradigm for synchronization phenomena. *Reviews of modern physics*, 77(1):137, 2005.

Supplemental Material for:

Nested hyperedges promote the onset of collective transitions but suppress explosive behavior

Federico Malizia,¹ Andrés Guzmán,² Federico Battiston,¹ and István Z. Kiss^{2,3}

¹ Department of Network and Data Science, Central European University, Vienna, Austria

² Network Science Institute, Northeastern University London, London E1W 1LP, United Kingdom

³ Department of Mathematics, Northeastern University, Boston, MA 02115, USA

SUPPLEMENTARY SECTION I: EFFECTS OF NESTEDNESS ON KURAMOTO DYNAMICS

To test the generality of the mechanisms identified for epidemic dynamics, we study synchronization in a system of phase oscillators with higher-order interactions on hypergraphs with tunable nestedness. The purpose of this section is not to develop a microscopic theory for synchronization, but rather to demonstrate that nested hyperedges produce the same qualitative effects observed for SIS dynamics: anticipation of the onset and suppression of discontinuous (explosive) transitions.

We consider a Kuramoto model with pairwise and three-body interactions, originally introduced in Ref. [30]. The dynamics of the phase $\theta_i(t)$ of oscillator i is given by

$$\dot{\theta}_i = \omega_i + \frac{\sigma_1}{k_1} \sum_{j=1}^N a_{ij}^{(1)} \sin(\theta_j - \theta_i) + \frac{\sigma_2}{2k_2} \sum_{j,k=1}^N a_{ijk}^{(2)} \sin(\theta_j + \theta_k - 2\theta_i), \quad (\text{S1})$$

where ω_i are natural frequencies drawn from a symmetric unimodal distribution, $a_{ij}^{(1)}$ is the adjacency matrix of the pairwise layer, and $a_{ijk}^{(2)}$ is the adjacency tensor encoding three-body interactions. The parameters σ_1 and σ_2 control the strength of pairwise and higher-order coupling, respectively, while k_1 and k_2 denote the average numbers of incident 1- and 2-hyperedges. The factor $1/(2k_2)$ avoids double counting of triadic contributions.

Synchronization is quantified by the standard Kuramoto order parameter

$$r(t) = \frac{1}{N} \left| \sum_{j=1}^N e^{i\theta_j(t)} \right|, \quad (\text{S2})$$

which ranges from $r = 0$ (incoherent state) to $r = 1$ (fully synchronized state). In contrast to epidemic dynamics, $r(t)$ typically exhibits persistent temporal fluctuations even in the synchronized regime. Therefore, for each realization we measure the time-averaged order parameter

$$\langle r \rangle = \frac{1}{\Delta t} \int_{t_r}^{t_r + \Delta t} r(t) dt, \quad (\text{S3})$$

where t_r is a transient time and Δt is taken sufficiently large to ensure convergence. Reported values correspond to the median of $\langle r \rangle$ over an ensemble of realizations. In the absence of higher-order interactions ($\sigma_2 = 0$), the model reduces to the standard Kuramoto dynamics on networks, which displays a continuous synchronization transition at a critical coupling σ_1^* [33]. The inclusion of three-body interactions, instead, can induce bistability and explosive synchronization via a saddle-node bifurcation, as shown in Ref. [30].

As in the SIS case discussed in the main text, we study this model on random regular hypergraphs with fixed (k_1, k_2) and tunable inter-order hyperedge overlap α , generated using the rewiring procedure described in Supplementary Section III. The parameter α controls the fraction of pairwise interactions that are structurally embedded within 2-hyperedges, interpolating between independent interaction orders ($\alpha = 0$) and fully nested (simplicial) structures ($\alpha = 1$). For each parameter set $(\alpha, \sigma_1, \sigma_2)$, we perform $M = 200$ simulations on synthetic regular hypergraphs with $N = 300$ nodes, half initialized with narrowly distributed phases and half with random phases uniformly distributed in $[0, 2\pi]$. For each run, we compute $\langle r \rangle$ and take the median over realizations.

In Supplementary Figure S1 we summarize the numerical results. Panel (a) reports the critical pairwise coupling σ_1^* marking the onset of synchronization, together with the critical three-body coupling $\hat{\sigma}_2$ required for the emergence of bistability, both as functions of the inter-order overlap α .

Specifically, for a fixed α , we determine $\hat{\sigma}_2$ and σ_1^* directly from the simulated forward and backward continuations of $\langle r \rangle(\sigma_1)$. Unlike the SIS case, where our mean-field theory and center-manifold analysis provide analytical conditions for both

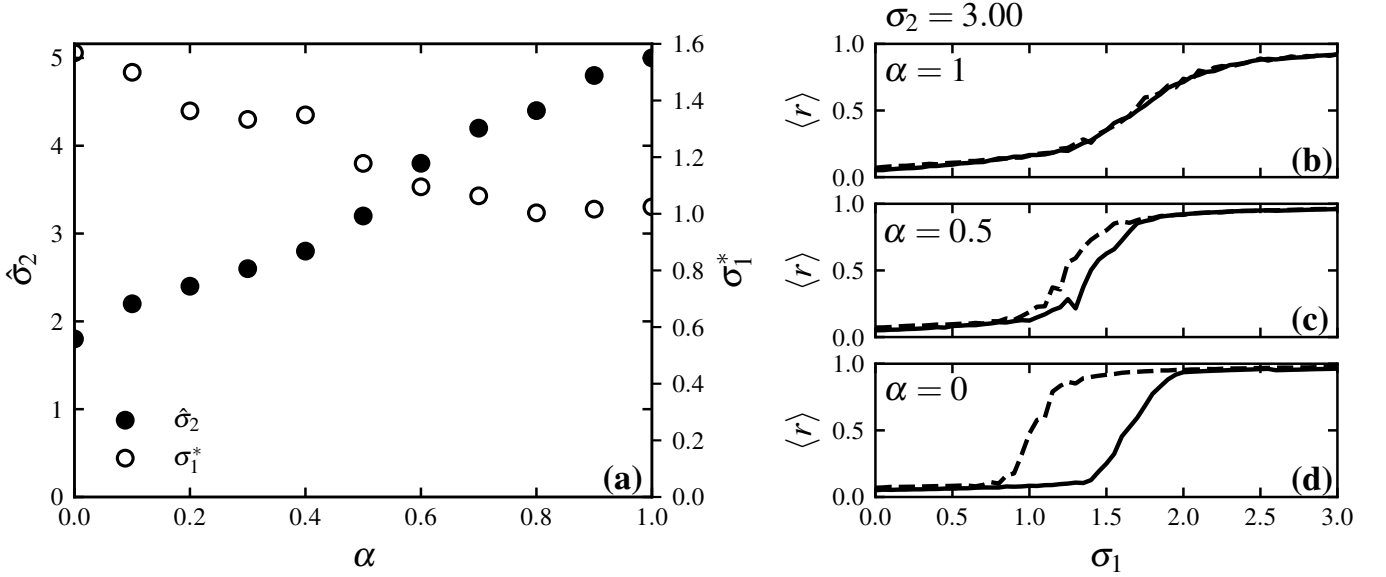


FIG. S1. **Nested hyperedges shape synchronization onset and explosive behavior in Kuramoto dynamics.** (a) Critical pairwise coupling $\hat{\sigma}_1^*$ (circles) and critical three-body coupling $\hat{\sigma}_2$ (filled symbols) as functions of the inter-order overlap α , obtained numerically from simulations on regular hypergraphs with $N = 300$, $k_1 = 5$, and $k_2 = 2$. (b-d) Time-averaged Kuramoto order parameter $\langle r \rangle$ as a function of σ_1 for $\sigma_2 = 3$ and $\alpha = 1, 0.5$, and 0, respectively. Solid (dashed) lines correspond to forward (backward) continuation. Increasing nestedness anticipates the synchronization onset while progressively suppressing bistability and explosive synchronization.

the onset and the bistability threshold, here we do not have a closed theory capturing the effect of nested hyperedges on Kuramoto dynamics; therefore, both quantities are extracted numerically.

For each α and each sampled value of σ_2 , we compute two branches: a *forward* branch $\langle r \rangle_f(\sigma_1)$ obtained by adiabatically increasing σ_1 along the grid (using the final state at the previous σ_1 as initial condition), and a *backward* branch $\langle r \rangle_b(\sigma_1)$ obtained by decreasing σ_1 analogously. To quantify the presence of bistability at a given (α, σ_2) , we measure the positive gap between the two branches and integrate it over σ_1 :

$$\mathcal{A}(\alpha, \sigma_2) \equiv \int \max\{ \langle r \rangle_b(\sigma_1) - \langle r \rangle_f(\sigma_1), 0 \} d\sigma_1, \quad (\text{S4})$$

which we evaluate numerically by trapezoidal integration on the σ_1 grid. We then define $\hat{\sigma}_2(\alpha)$ as the smallest σ_2 for which $\mathcal{A}(\alpha, \sigma_2)$ exceeds a small threshold, and we additionally impose a minimal ‘‘real gap’’ condition to avoid spurious detections due to finite-size noise: we require that the forward branch stays below a low value $\langle r \rangle_f \leq r_{\text{low}}$ while the backward branch is simultaneously above a higher value $\langle r \rangle_b \geq r_{\text{high}}$ for at least a few consecutive σ_1 points.

Once $\hat{\sigma}_2(\alpha)$ is identified, we compute the corresponding synchronization onset $\sigma_1^*(\alpha)$ from the forward branch at $\sigma_2 = \hat{\sigma}_2(\alpha)$ as the first σ_1 where $\langle r \rangle_f(\sigma_1)$ crosses a small reference level $r_{\text{thr}} = 0.2$ (we use linear interpolation between adjacent grid points). This operational definition is robust to small oscillations in $\langle r \rangle$ and finite-size fluctuations, and it provides the Kuramoto analogue of the forward critical point λ_1^* used in the SIS analysis.

Panels (b-d) show representative phase diagrams $\langle r \rangle$ versus σ_1 for $\sigma_2 = 3$ and three values of α . For $\alpha = 1$ [panel (b)], the transition is continuous and forward and backward branches coincide. At intermediate overlap [panel (c)], a bistable region emerges, while for $\alpha = 0$ [panel (d)] the bistability window is maximal, signaling explosive synchronization. Increasing nestedness systematically shifts the onset of synchronization to smaller σ_1 while simultaneously suppressing bistability.

Overall, these results demonstrate that nested hyperedges have the same qualitative impact on synchronization as on epidemic spreading: they anticipate the linear onset of collective behavior while suppressing discontinuous transitions. This strong phenomenological correspondence supports the generality of our findings and suggests that the role of nested higher-order interactions in shaping collective dynamics extends well beyond contagion processes.

SUPPLEMENTARY SECTION II: DERIVATION OF THE ANALYTICAL FAST VARIABLES

We derive the quasi-stationary (early-time) values of the fast variables $\Pi \equiv \rho^{\text{SI}}/\rho^{\text{I}}$ and $\delta \equiv \rho^{\text{ISI}\Delta}/\rho^{\text{SI}}$ by exploiting time-scale separation close to the disease-free equilibrium. In the regime $\rho^{\text{I}} \rightarrow 0$, node density ρ^{I} evolves slowly, while pair and group

motif densities rapidly relax to values that are slaved to ρ^I . Accordingly, we treat ρ^I as quasi-constant and impose $\dot{\rho}^{SI} \simeq 0$ and $\dot{\rho}^{ISI\Delta} \simeq 0$ (and, when needed, $\dot{\rho}^{SSI\Delta} \simeq 0$), retaining only the leading-order contributions in ρ^I .

We start from the closed mean-field system reported in Appendix A. Close to the disease-free state, the relevant variables scale as $\rho^{SI}, \rho^{SSI\Delta}, \rho^{ISI\Delta} = \mathcal{O}(\rho^I)$, while $\rho^S = 1 - \rho^I = 1 + \mathcal{O}(\rho^I)$ and $\rho^{SS\Delta} = 1 + \mathcal{O}(\rho^I)$. All composite terms are closed using the same factorized approximations of the main text, e.g., $\rho^{ISI} \approx (\rho^{SI})^2/\rho^S$, $\rho^{SSI} \approx \rho^{SS}\rho^{SI}/\rho^S$, $\rho^{IIS\Delta I} \approx \rho^{ISI\Delta}\rho^{SI}/\rho^S$, $\rho^{IIS\Delta S} \approx \rho^{ISI\Delta}\rho^{SS}/\rho^S$, and similarly for the remaining composite motifs.

Step 1: quasi-stationary ratio $\bar{\delta} = \rho^{ISI\Delta}/\rho^{SI}$. At leading order, $\dot{\rho}^{ISI\Delta} = 0$ yields a linear relation between $\rho^{ISI\Delta}$ and ρ^{SI} , because all quadratic terms (e.g., involving products of two $\mathcal{O}(\rho^I)$ quantities) can be neglected. Using $\rho^{SSI\Delta} = \mathcal{O}(\rho^I)$ and the closure $\rho^{IIS\Delta I} \approx \rho^{ISI\Delta}\rho^{SI}$ and $\rho^{IIS\Delta S} \approx \rho^{ISI\Delta}$ (since $\rho^{SS} \simeq 1$), the dominant balance in $\dot{\rho}^{ISI\Delta}$ can be written as

$$0 \simeq \beta_1 \alpha k_2 \lambda_1^{*2} \frac{k_1 - 2\alpha}{k_1} \rho^{SI} - \beta_2 \alpha \lambda_1^* \lambda_2 (k_2 - 1) \rho^{ISI\Delta} - k_1 k_2 \rho^{ISI\Delta},$$

where we have used the rescaled infectivities $\lambda_1 = k_1 \beta_1 / \mu$ and $\lambda_2 = k_2 \beta_2 / \mu$ and evaluated the expression at the epidemic threshold $\lambda_1 = \lambda_1^*$. Solving for $\rho^{ISI\Delta}/\rho^{SI}$ gives the quasi-stationary value

$$\bar{\delta} \equiv \frac{\rho^{ISI\Delta}}{\rho^{SI}} = \frac{\alpha k_2 \lambda_1^{*2} (k_1 - 2\alpha)}{k_1 [k_1 k_2 - \alpha \lambda_1^* \lambda_2 (k_2 - 1)]},$$

which coincides with Eq. (??) in the main text. This expression immediately implies $\bar{\delta} = 0$ for $\alpha = 0$, i.e., triadic transmission does not contribute at early times without nestedness.

Step 2: quasi-stationary ratio $\bar{\Pi} = \rho^{SI}/\rho^I$. We next impose $\dot{\rho}^{SI} \simeq 0$ and keep only leading terms in ρ^I . Near the disease-free state, we use $\rho^{II} = \rho^I - \rho^{SI} = \mathcal{O}(\rho^I)$ and the pair closures $\rho^{SSI} \approx \rho^{SS}\rho^{SI}/\rho^S \simeq \rho^{SI}$ and $\rho^{ISI} \approx (\rho^{SI})^2/\rho^S = \mathcal{O}((\rho^I)^2)$, so that terms involving ρ^{ISI} are negligible at leading order. For the cross-order contributions, we express $\rho^{ISI\Delta} = \bar{\delta} \rho^{SI}$ and retain only terms linear in ρ^{SI} . This yields a linear balance of the form

$$0 \simeq -\mu \rho^{SI} + \beta_1 \left[(k_1 - 1) \rho^{SI} - \rho^{SI} \right] + \beta_2 \frac{k_2}{k_1} \left[(k_1 - 2\alpha) \rho^{ISI\Delta} - 2\alpha \rho^{ISI\Delta} \right] + \mu (\rho^{II} - \rho^{SI}),$$

which, after substituting $\rho^{II} = \rho^I - \rho^{SI}$ and $\rho^{ISI\Delta} = \bar{\delta} \rho^{SI}$, can be rearranged to obtain ρ^{SI}/ρ^I . Evaluated at $\lambda_1 = \lambda_1^*$, the resulting quasi-stationary value is

$$\bar{\Pi} \equiv \frac{\rho^{SI}}{\rho^I} = \frac{k_1}{2k_1 - \lambda_1^* (k_1 - 2) + \lambda_2 (4\alpha - k_1) \bar{\delta}},$$

again matching the results shown in the main text. Finally, since $\Psi \equiv \rho^{ISI\Delta}/\rho^I = \delta \Pi$, we also have $\bar{\Psi} = \bar{\delta} \bar{\Pi}$.

Together, Π and $\bar{\delta}$ quantify the early-time balance between dyadic and triadic contagion channels and provide a mechanistic decomposition of how nested hyperedges reshape the onset of spreading.

SUPPLEMENTARY SECTION III: HIGHER-ORDER NETWORKS WITH VARYING LEVELS OF INTER-ORDER HYPEREDGE OVERLAP

In this work we consider regular higher-order networks with interactions up to order $M = 2$, where each node participates in exactly k_1 pairwise interactions (1-hyperedges) and k_2 three-body interactions (2-hyperedges). We describe here the numerical procedure used to generate ensembles of such hypergraphs with controlled nestedness, quantified by the inter-order hyperedge overlap α .

We first generate a set of 2-hyperedges such that each node belongs to exactly k_2 three-body interactions. This is achieved using configuration-model-like procedures for regular hypergraphs with $M = 2$, discarding realizations containing self-loops or repeated hyperedges. Once generated, the set of 2-hyperedges is kept fixed throughout the entire construction.

Given the set of 2-hyperedges, we construct an initial configuration of 1-hyperedges that is maximally nested inside them, corresponding to $\alpha = 1$. In this fully nested configuration, all pairwise interactions are embedded within 2-hyperedges and the structure forms a simplicial complex. Since each 2-hyperedge contributes three internal links, the maximum admissible value of the pairwise degree is bounded by $k_1 \leq (k_2 - 1)(k_2 - 2)/2$. For admissible values of (k_1, k_2) , we select k_1 internal links per node from those induced by the 2-hyperedges, ensuring regularity of the pairwise degree.

Starting from this fully nested configuration, we generate hypergraphs with lower values of α by applying a numerical rewiring procedure to the set of 1-hyperedges, while keeping both k_1 and k_2 fixed. At each iteration, two distinct 1-hyperedges are selected at random and one endpoint from each link is chosen. The selected endpoints are swapped, producing two new candidate links.

The swap is accepted if no multiple links are created and if the resulting inter-order hyperedge overlap α does not increase; otherwise, the original configuration is retained. By iterating this procedure, the fraction of pairwise links embedded within 2-hyperedges is progressively reduced, allowing us to explore the full range $\alpha \in [0, 1]$ while preserving the regularity of the hypergraph. Importantly, throughout this process the set of 2-hyperedges remains unchanged.

Using this method, we generate ensembles of regular higher-order networks with identical values of (k_1, k_2) but different degrees of nestedness. These ensembles are used consistently for both SIS and Kuramoto dynamics, allowing us to isolate the effects of nested hyperedges from those induced by degree heterogeneity or intra- and cross-order degree correlations.